



Modified regional biogenic VOC emissions with actual ozone stress and integrated land cover information: A case study in Yangtze River Delta, China

Yutong Wang^a, Yu Zhao^{a,b,*}, Lei Zhang^a, Jie Zhang^c, Yang Liu^d

^a State Key Laboratory of Pollution Control and Resource Reuse and School of the Environment, Nanjing University, 163 Xianlin Ave., Nanjing, Jiangsu 210023, China

^b Jiangsu Collaborative Innovation Center of Atmospheric Environment and Equipment Technology (CICAEET), Nanjing University of Information Science and Technology, Jiangsu 210044, China

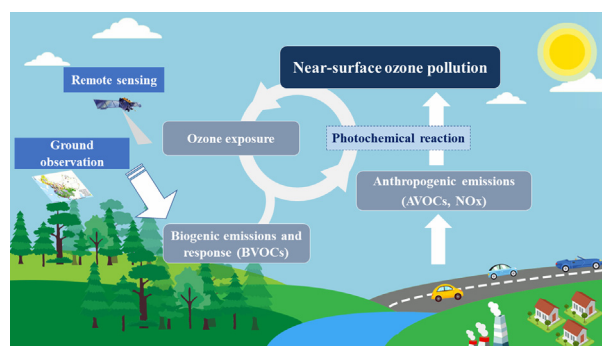
^c Jiangsu Provincial Academy of Environmental Science, 176 North Jiangdong Rd., Nanjing, Jiangsu 210036, China

^d Department of Environmental Health, Emory University, Rollins School of Public Health, Atlanta, GA 30322, United States

HIGHLIGHTS

- Actual ozone exposure was included in the estimation of BVOCs emissions.
- Isoprene emissions were inhibited along the Yangtze River due to ozone exposure.
- Applying global emission factors underestimated the isoprene emissions in YRD.
- Land cover data influenced greatly the isoprene emission estimation in summer.
- NO_x emissions were closely related with the contribution of isoprene to O₃ formation.

GRAPHICAL ABSTRACT



ARTICLE INFO

Article history:

Received 19 February 2020

Received in revised form 12 April 2020

Accepted 13 April 2020

Available online 17 April 2020

Editor: Jianmin Chen

Keywords:

Isoprene

Ozone

Exposure-response function

MEGAN

Air quality

ABSTRACT

The biogenic volatile organic compounds (BVOCs) emissions are influenced by ambient ozone (O₃) concentrations and vegetation cover. In most studies, however, the interaction between O₃ and plants has not been considered and there are uncertainties in land cover input and emission factors (EFs) in BVOCs emission estimation, particularly at the regional scale. In this study, an O₃ exposure-isoprene (ISOP) response function was developed using meta-analysis, and the EFs of ISOP and land cover inputs were updated by integrating local measurement and investigation data in the Yangtze River Delta (YRD) region. Five different cases were developed to explore the impacts of O₃ and input variables on the BVOCs emissions using the Model of Emissions of Gases and Aerosols from Nature (MEGAN). The impacts of those variables on O₃ simulation were further examined with air quality modeling. We found that the ISOP emissions were restrained in the city cluster along the Yangtze River during the growing season due to their negative feedback to O₃ exposure for deciduous broadleaf forests. The estimation of BVOCs emissions strongly depended on EFs, and the global EFs underestimated the ISOP emissions in July by 37%, mostly in southern YRD. Different land cover datasets with various fractions and spatial distributions of plant function types resulted in a variation of 200–400 Gg in ISOP emissions in July across YRD. Air quality modeling indicated that BVOCs contributed 10%, 12%, and 11% to the 1-h mean, the maximum daily 1-h average, and the maximum daily 8-h average O₃

* Corresponding author at: State Key Laboratory of Pollution Control and Resource Reuse and School of the Environment, Nanjing University, 163 Xianlin Ave., Nanjing, Jiangsu 210023, China.

E-mail address: yuzhao@nju.edu.cn (Y. Zhao).

concentrations, respectively, for July across the YRD region. Due to the NO_x restriction, the spatial distribution of BVOCs emissions was inconsistent with that of their contribution to O₃ formation. The O₃ simulation was more sensitive to the changed BVOCs emissions in the area with relatively large contribution of BVOCs to O₃ formation.

© 2020 Elsevier B.V. All rights reserved.

1. Introduction

Biogenic volatile organic compounds (BVOCs) from terrestrial forests are identified as a strong link between the earth surface and the atmosphere (Laothawornkitkul et al., 2009). Accounting for approximately 90% of emissions, biogenic sources serve as the dominant contributor to global VOCs (Guenther et al., 2012). The most abundant species of BVOCs are isoprene (ISOP) and monoterpene (MON). With a strong chemical reactivity, they can be oxidized by hydroxyl radicals (OH) and influence the oxidation capacity of the atmosphere (Gong et al., 2018), resulting in enhanced formation of ozone (O₃) and secondary organic aerosols (SOAs) (Geng et al., 2011; Paasonen et al., 2013; Shilling et al., 2013). Given their importance in atmospheric chemistry, models have been developed to estimate BVOCs emissions (Guenther et al., 1995; Niinemets et al., 1999; Arneeth et al., 2007; Guenther et al., 2012), and are further incorporated into chemical transport modeling to examine the impact of BVOCs on air quality and climate change (von Kuhlmann et al., 2004; Xie et al., 2007; Lou et al., 2010; Unger, 2014). Through a sensitivity analysis, for example, von Kuhlmann et al., 2004 found that the abundance of peroxyacetyl nitrate was significantly reduced when the ISOP emission strength declined by 50% at the global scale.

The Model of Emissions of Gases and Aerosols from Nature (MEGAN) has commonly been used to estimate the BVOCs emissions in different regions (Li et al., 2013; Sindelarova et al., 2014; Wang et al., 2016; Liu et al., 2018; Chen et al., 2018). It is a statistical model that depends on the basal emission rate and leaf area index (LAI), and it can be further modulated with an improved understanding of the BVOCs responses to environmental factors and plant physiological conditions. However, considerable uncertainties exist in MEGAN, attributed to incorrect or incomplete information on the ambient air pollution level (e.g., O₃ exposure), land cover and basal emission rate by vegetation type (Guenther et al., 2012). The influences of those factors were not well quantified, and the bias in BVOCs emission estimation remained unclear at regional scale.

Ignoring the response of BVOCs emissions to O₃ exposure is one source of uncertainty in MEGAN. Tropospheric O₃ is a phytotoxic pollutant, which poses a considerable threat to human health and plant physiology. Peak O₃ concentrations can not only lead to leaf damage and growth inhibition but also influence the synthesis and release of secondary metabolites including BVOCs (Feng and Yuan, 2018). Given the importance of BVOCs in photochemical processes, studies have been conducted to examine the O₃ impacts on BVOCs synthesis, but most of them have focused only on one vegetation species, and the findings are controversial (Penuelas and Staudt, 2010). The discrepancy resulted from the various plant types and O₃ exposure levels across studies. For example, Velikova et al. (2005) claimed that the ISOP emissions from Mediterranean oak species were stimulated by elevated O₃ exposure during three consecutive days. However, Yuan et al. (2017) found that chronic O₃ fumigation significantly inhibited the ISOP emissions from *Poplar*. To date, the feedback of BVOCs to O₃ exposure has not been well described, and there are few comprehensive O₃ exposure-BVOCs response functions in current emission models (Penuelas and Staudt, 2010; Tiwari et al., 2016). As high O₃ concentrations usually occur in the plant growing seasons including spring and summer (Wang et al., 2017; Feng and Yuan, 2018), a reasonable O₃ exposure-BVOCs response function is essential for better estimating the BVOCs emissions.

In addition to O₃ exposure, basal emission rates and land use data also serve as major contributors to the overall uncertainty of BVOCs emissions (Guenther et al., 2012). For example, underestimation in the ISOP emissions from the bottom-up methods in eastern China was commonly suggested by the top-down estimates based on the satellite and aircraft observations (Shim et al., 2005; Fu et al., 2007; Warneke et al., 2002; Marais et al., 2012; Stavrou et al., 2014). Most studies adopted the default emission factors (EFs) in MEGAN that represent the global average level, while field measurements combined with local vegetation composition data could result in diverse EFs for specific areas. Li, 2015 found that the ISOP emissions estimated based on global EFs were half of those based on local EFs in China. The estimation of BVOCs emissions can also be affected by the inconsistent land cover information in various datasets or satellite products. At the regional scale, particularly, different satellite sensors and classification systems cause significant discrepancies in the land use distribution. Besides, the land use in complex terrains might not be well captured due to the limited identification capability of satellite sensor, and the inaccurate information would lead to bias in emission estimation. Wang et al. (2018) suggested that different satellite products can result in a variation of ~20 Gg in the annual BVOCs emissions in Beijing, indicating the necessity of carefully examining the land cover information from various datasets.

The Yangtze River Delta (YRD) is a typical developed region in eastern China, with mixed sources of air pollutants and poor air quality (Li et al., 2019). Located in the subtropics, the southern YRD has abundant broadleaf vegetation, one of the main contributors to ISOP emissions, and its coverage was reported to have grown in recent years (Zhejiang Forestry Administration, <http://www.zjly.gov.cn/>), enhancing the potential of the BVOCs emissions in the region. Due to the high emissions of anthropogenic VOCs (AVOCs) and gradually reduced particle pollution, the O₃ concentrations in the YRD region were observed to increase at an average rate of 2.3 ppbv a⁻¹ from 2013 to 2017 (Li et al., 2019), and the elevated O₃ exposure was expected to play an important role on BVOCs emissions. These changing factors make it quite challenging in estimating BVOCs emissions. Current available studies, however, commonly adopted the land cover information and basal emission rates for earlier period (2000–2010) and ignored the feedback of BVOCs to O₃ exposure in the YRD, resulting in potentially large uncertainties (Song, 2012; Li et al., 2016; Liu et al., 2018). Due to the high levels of ambient NO_x from anthropogenic emissions, the YRD region has gradually transitioned from a NO_x-limited regime to a mixed or VOC-limited regime in terms of O₃ formation (Jin and Holloway, 2015), indicating the elevated impacts of VOCs (including BVOCs) on the ambient O₃ level. Therefore, a comprehensive analysis on the influences of method and data on BVOCs emission estimation is in great need for better understanding the roles of biogenic sources on regional air quality.

In this study, we modified the BVOCs emissions considering the actual O₃ stress and integrating the land cover information in the YRD region. We developed and applied a scheme of O₃-ISOP linkage in MEGAN based on meta-analysis of available experiments on the response of ISOP emissions to O₃ exposure. A set of local ISOP EFs was obtained by combining the distribution of vegetation types and updated field measurements in China. Satellite products and ground surveys were integrated to correct the land cover and vegetation distribution information. The impacts of the main factors on BVOCs emissions and

O₃ formation were then diagnosed through sensitivity simulations in MEGAN and an air quality model.

2. Methodology and data

2.1. Model description

We estimated the BVOCs emissions in the YRD region for 2015 with MEGAN version 2.1. The model quantifies the average land EFs and the response of BVOCs emissions to environmental conditions (Guenther et al., 2012):

$$E_i = \gamma_i \sum \varepsilon_{i,j} \chi_j \quad (1)$$

where E_i is the emissions of compound category i ($\mu\text{g m}^{-2} \text{h}^{-1}$), and four main categories were included (ISOP, MON, sesquiterpene (SQT) and other VOCs); $\varepsilon_{i,j}$ is the EF of compound category i under standard conditions for vegetation type j (described in Section 2.3); and χ_j is the grid area proportion of vegetation type j (described in Section 2.4). The activity factor γ_i accounts for the impacts of environmental and phenological conditions on BVOCs emissions and was calculated as:

$$\gamma_i = LAI \gamma_{CE} \gamma_{P,i} \gamma_{T,i} \gamma_{age,i} \gamma_{SM} \gamma_C \quad (2)$$

where LAI accounts for the leaf density in each grid and the data were obtained from Global Land Surface Satellite (<http://www.geodata.cn/thematicView/GLASS.html>); γ_{CE} is the canopy environmental coefficient, assigned a value of 0.57 in MEGAN; $\gamma_{P,i}$ and $\gamma_{T,i}$ account for the light and temperature responses of emissions respectively, driven by the meteorological fields with the Weather Research and Forecasting Model (WRF, described later in this section); $\gamma_{age,i}$ is the leaf age correction factor, associating with variation of LAI in a certain period; γ_{SM} captures the effect of soil moisture; and γ_C describes the effect of carbon dioxide (CO₂) on ISOP. The impacts of the soil moisture and CO₂ concentrations on BVOCs emissions were not considered in this work by setting $\gamma_{SM}=1$ and $\gamma_C=1$.

The O₃ concentrations were simulated with the Models-3 Community Multiscale Air Quality (CMAQ) version 5.1 (Wyat Appel et al., 2017). As shown in Fig. S1 in the supplement, we adopted the Lambert Conformal Conic projection centered at (110° E, 34° N), and two-nested-domain simulations with horizontal resolutions of 27 km and 9 km were conducted. The first domain (D1, 177 × 127 cells) covered most of China, and the second domain (D2, 118 × 121 cells) covered the YRD region, including the provinces of Jiangsu, Zhejiang, and Anhui, and the city of Shanghai. We adopted the carbon bond gas-phase mechanism (CB05) for VOCs and AERO6 for the particulate matter. The initial and boundary conditions for the first domain were set as the clean continental conditions provided by CMAQ.

The anthropogenic emissions in D1 were obtained from the Multi-resolution Emission Inventory for China (MEIC, <http://www.meicmodel.org/>, Zheng et al., 2018) with a spatial resolution of 0.25° × 0.25°. Developed by Tsinghua University, MEIC provided the national emission estimates integrating the unit-based power plant emission model (Liu et al., 2015), the high-resolution on-road vehicle emission model (Zheng et al., 2014), and the comprehensive NMVOC chemical speciation model (Li et al., 2014). The emission data from MEIC were further allocated to D2 based on the gross domestic product (GDP) per capita and population density. Biogenic emissions were generated with MEGAN, and the Cl and HCl emissions were obtained from the Global Emissions Initiative (GEIA, Price et al., 1997).

The Weather Research and Forecasting Model (WRF) version 3.4 (Skamarock et al., 2008) was applied to provide the meteorological fields in this study. The WRF input data were obtained from the National Centers for Environmental Prediction (NCEP) FNL Operational Model Global Tropospheric Analyses datasets (<https://rda.ucar.edu/datasets/>). Detailed WRF model configurations are as described in Fu et al.

(2013). We evaluated the WRF model performance with the observation data obtained from the National Climatic Data Center (<https://gis.ncdc.noaa.gov/>) at 42 ground stations in D2 (as shown in Fig. S1). Fig. S2 in the supplement compares the averages of the simulated and observed temperatures at 2 m (T2), relative humidity at 2 m (RH2), and wind speed and direction at 10 m (WS10 and WD10), for January, April, July and October 2015. The evaluation indicators, including bias, index of agreement (IOA), root mean square error (RMSE) and R², are summarized in Table S1 in the supplement. The discrepancies between the ground observations and WRF modeling results were within an acceptable range (Emery et al., 2001).

2.2. Exposure-response function between ISOP emissions and ambient O₃ level

2.2.1. Data collection

We compiled a database containing the responses of BVOCs emissions to O₃ exposure by investigating the peer-reviewed publications with the Web of Science (ISI). Using “ozone”, “O₃”, “VOC”, “BVOC”, “forest”, “tree”, “woody”, and “plant” as keywords, we collected 77 papers in total published between 1990 and 2018. In most of the collected studies, experimental plants were chronically exposed to O₃ using growth chambers, open-top chambers, branch chambers, or other fumigation methods. Those studies suggested that high O₃ level can not only lead to leaf damage and growth inhibition, but also affect the synthesis and release of plant secondary metabolites by interfering with photosynthesis and inducing defensive feedback mechanisms. Measurement data were excluded if (a) parallel experiments were not conducted and the standard deviation was unclear; (b) the experiment period was shorter than seven days and the experiment could not be considered as a chronic fumigation experiment; (c) there were other environmental factors in addition to O₃ included in the studies so that the single effect of O₃ was unclear; (d) the BVOCs emission rate, O₃ concentration and fumigating duration were not reported clearly; or (e) the O₃ concentration was lower than the threshold value (40 ppb). Relevant information from the remaining measurements was collected, including plant species, O₃ concentration or O₃ exposure level, fumigating duration, and control and experimental ISOP emission rates. In total, 93 data pairs of O₃ exposure levels and relative ISOP emission rates across 15 studies were obtained for the meta-analysis, as summarized in Table S2 in the supplement.

2.2.2. Meta-analysis

To assess the O₃ impact on plants over a period of time, we chose the O₃ index (AOT40, i.e., the accumulated exposure to hourly O₃ concentration above 40 ppb) as the predictor variable. Although some researchers suggested that flux-based metrics (e.g., POD_y, i.e., the phytotoxic O₃ dose over threshold y in $\text{nmol O}_3 \text{ m}^{-2} \text{ s}^{-1}$) could better represent the uptake of O₃ by plants and physiological damage over time, AOT40 was adopted in this work because there were few data on the O₃ flux in the currently available studies. AOT40 was directly used if it was available in the published study (there were 6 studies reporting AOT40); otherwise, it was calculated using the O₃ concentration and exposure duration data reported in the study. For a specific experiment containing more than three measurements, the ISOP emission rate without O₃ exposure was determined as the intercept of the linear regression line of the AOT40 and ISOP emission rates. AOT40 was calculated as:

$$\text{AOT40 (ppb h)} = \int_{t=1}^n \max((O_3 - 40), 0) dt \quad (3)$$

where O_3 is the O₃ concentration (ppb) at which trees are exposed during the daytime (7:00–19:00) in the growing season from April to September; and t is the exposure duration (hour).

We used linear regression to analyze the relationship between the relative emission rate (RE, defined as the ratio of the ISOP emission rate at a certain exposure level of O₃ to that without O₃ exposure) and AOT40. Kolmogorov-Smirnov test was used to evaluate whether the response variables were normally distributed. Regressions were considered statistically significant at a *P* value < 0.05.

2.3. Emission factor

In addition to the default global average EFs in MEGAN, a set of local EFs of ISOP was developed in this work to modify the BVOCs emissions. Due to a lack of data, the EFs for compounds other than ISOP were not modified, and default global ones were still adopted. The standard canopy-scale EF (μg/m² h) for each plant function type (PFT) can be converted by the measured leaf-scale emission rate (μg C/gdw h) and leaf biomass density (gdw/m²) of the vegetation species in the PFT. Because there are various emission rates for a specific species, the EF of ISOP by PFT is calculated as follows:

$$\varepsilon_j = \sum \varphi_k LMA_k \frac{s_k}{s_j} \quad (4)$$

where ε_j is the standard EF for PFT *j* (μg/m² h), φ_k is the standard emission rate for vegetation species *k* (μg C/gdw h), LMA_k is the leaf biomass density for vegetation species *k*, s_k is the area occupied by vegetation species *k*, and s_j is the area occupied by PFT *j*.

In this work, the local emission rates and leaf biomass densities by species were obtained from previous publications (Song, 2012, Li, 2015, Wang et al., 2018). If exact information was unavailable, the approximate values for species within the same genus and family were adopted. The area fractions of the species were derived from the Vegetation Atlas of China (1:1,000,000) (Data source: Resource Discipline Innovation Platform, Chinese Academy of Sciences). The detailed EFs, area fractions and leaf biomass densities are summarized in Tables S3 and S4 in the supplement.

2.4. Land cover

Satellite remote sensing is an important tool for detecting the land cover information, especially for a broad area with a high horizontal resolution. There are many land cover datasets derived from various satellite observations. In this work, we chose the Moderate-Resolution Imaging Spectroradiometer (MODIS) MCD12Q1 and Climate Change Initiative (CCI) products as the vegetation input data for MEGAN. Both products have been widely applied in estimating the BVOCs emissions and examining the influence of vegetation change on the ambient levels of atmospheric components due to their high resolutions, detailed land use classifications and wide ranges of time and space (Fu and Liao, 2012; Fu and Liao, 2014; Fu and Tai, 2015; Wang et al., 2016; Chen et al., 2019).

With the finest horizontal resolution at 500 m, MODIS operates on both Terra and Aqua satellite, and the data products are derived from six different classification schemes. We directly used the PFT map layer of the MCD12Q1 product with 12 land cover types because it meets the input requirements in MEGAN. The CCI was launched by the European Space Agency, and its product with a horizontal resolution of 300 m classifies the land cover into 22 types following the legend of the United Nations Land Cover Classification Scheme. We used the cross-walking table provided by Poulter et al. (2015) to convert land cover types into PFTs. The benchmark years of MODIS and CCI were both set at 2015.

Given the considerable uncertainties of the satellite datasets (Wu et al., 2009), we also developed a more reliable land cover dataset for the YRD region (labeled MULTI) by integrating land use and land cover change (LUCC), MODIS MCD12Q1 and Vegetation Atlas data with plant statistics in China. The LUCC data for 2015 was provided by the Data Center for Resources and Environmental Sciences, Chinese

Academy of Sciences (RESDC, <http://www.resdc.cn>). Based on remote sensing images such as Landsat 8 OLI and GF-2, LUCC data were mainly obtained through a high-resolution remote sensing–unmanned aerial vehicle–ground survey observation system (Ning et al., 2018). There are 6 land cover classes at Level I and 25 classes at Level II in the dataset with a horizontal resolution of 1 km at the national scale. We chose the LUCC dataset as the basis because it has been validated by field surveys and aerial images with a high accuracy, as reported by Ning et al. (2018). We aggregated the 25 land cover classes at Level II into 7 land cover types, including crop, forest, shrub, grass, water, urban and rural land, and unused land. We performed spatial intersection of the LUCC and MCD12Q1 data using the pixel-by-pixel contrast method to subdivide the LUCC forest data. The forests were divided into evergreen broadleaf, deciduous broadleaf and needle trees by the MCD12Q1 data which has twelve PFTs. When a pixel had different land cover types in LUCC and MCD12Q1, we reclassified the pixel using the Vegetation Atlas of China with more detailed vegetation information.

2.5. O₃ exposure

We collected the monitored data of hourly O₃ concentrations for the YRD region in 2015. The data were obtained from the National Monitoring Network (215 state-operating sites, <http://113.108.142.147:20035/emcpublish/>) and the Jiangsu Provincial Atmospheric Automatic Monitoring and Warning Platform (48 sites, <http://58.213.159.173/Atmosphere/top.aspx>). In total, there were 263 observation sites available (as illustrated in Fig. S1) with a minimum data coverage of 95% for the whole growing season, and 159 and 104 were respectively located in urban and rural regions. Inclusion of the provincial-level sites partly corrected the bias in O₃ observation, particularly in the rural areas. The concentration was eliminated if it was negative or 200 μg/m³ larger than the contiguous ones. For the moments without measurement, the average of the concentrations 1 h before and after (if available) was applied to fill in the missing value. For the moments without continuous data at a given site, we set up a 30 km buffer zone around the site, and the average concentration for all the other sites within the buffer zone at the same moment was applied instead. We did not screen the anomalously low values, and the uncertainty was believed to be insignificant since the damage to vegetation occurs only at high O₃ concentrations. We performed Kriging interpolation on the hourly O₃ concentrations to obtain the spatial pattern of the O₃ concentration across the YRD region during the growing season.

2.6. Experiment description

We designed a series of WRF-MEGAN-CMAQ simulations to examine the sensitivities of BVOCs emissions and simulated O₃ concentrations to EFs, land cover and O₃ exposure, and to evaluate the contributions of biogenic sources to the O₃ concentrations. Table 1

Table 1

Summary of BVOC emission estimation cases in this study. Case 1 is the base case, and Cases 1 and 2 were used to explore the impact of O₃ stress. Cases 1 and 3 were used to investigate the impact of emission factors, and the influence of land cover was studied by Cases 1, 4, and 5. The contribution of BVOCs to O₃ was explored by Cases 2 and 6. T and F represent w/ and w/o the consideration of the factor, respectively.

Case	Research period (month)	BVOCs configuration			AVOCs ^a	
		EF	PFT	O ₃ stress	T	F
Case 1	January, April, July, October	LOCAL	MULTI	F	T	T
Case 2	January ^b , April, July, October	LOCAL	MULTI	T	F	T
Case 3	July	GLOBAL	MULTI	F	F	T
Case 4	July	LOCAL	CCI	F	F	T
Case 5	July	LOCAL	MODIS	F	F	T
Case 6	July	BVOCs removed			F	T

^a For the air quality modeling with CMAQ.

^b The same as Case 1.

summarizes the cases we applied. Without consideration of the influence of O₃ exposure on the BVOCs emissions, Case 1 is set as the baseline BVOCs emission case, applying local EFs and the integrated MULTI land cover dataset. The results of Cases 1 and 2 are compared to evaluate the impact of O₃ stress on ISOP emissions. January, April, July and October were selected as the representative months for the four seasons. As the vegetation growing period lasts from April to September in YRD, no extra effect of O₃ exposure was expected on BVOCs emissions for January resulting in the same emissions in Cases 1 and 2 for the month. We further selected July and set Cases 3–5 to evaluate the impacts of the EF and land cover data selection on BVOCs emission estimation, as no seasonal variation was assumed for the above two factors. The comparison between Cases 1 and 3 revealed the influence of EFs on BVOCs emission, and that among Cases 1, 4 and 5 revealed the influence of various land cover datasets. We further ran CMAQ by separately applying the BVOCs emission estimations of Cases 1–5, and the influences of the various inputs of BVOCs emissions on the O₃ simulations could be investigated. Moreover, we performed Case 6 in which the BVOCs emissions were removed, and the difference in simulated O₃ between Cases 2 and 6 indicated the contribution of BVOCs emissions to O₃ formation. July was selected for CMAQ modeling, as summer suffered the heaviest O₃ pollution in the YRD region (Wang et al., 2017). Furthermore, the uncertainty of BVOCs emissions was estimated to play a greater role on O₃ simulation in summer than in other seasons (Lou et al., 2010).

3. Results and discussions

3.1. Inhibition effect of O₃ on the ISOP emissions

3.1.1. The exposure-response function

The correlation between the relative emission rate of ISOP (RE) and AOT40 was analyzed for all 93 data pairs. Fig. 1a shows the relationships between RE and AOT40 by species, including *Quercus*, *Sphagnum moss*, *Pine*, *Poplar*, and *Ginkgo*. The RE for *Pine*, *Ginkgo*, and *Sphagnum moss* are larger than 1, indicating that O₃ exposure would elevate the ISOP emission rates of those species. However, most of the RE for *Poplar* and *Quercus* are smaller than 1, suggesting that their ISOP emissions were more likely to be inhibited by O₃ exposure. The average RE is calculated at 0.9574, and there is no correlation between RE and AOT40 for the whole dataset ($P > .05$), largely resulting from four data points with RE above 2.5. In addition, very large discrepancies existed in the relationships by species (Fig. 1a). Given the diverse responses of the species to O₃, we developed regression models for different PFTs. We chose the data for *Poplar*, *Quercus* and *Ginkgo* to establish the exposure-response function between RE and AOT40 for deciduous broadleaf trees. The exposure-response function for the other PFTs could not be developed

in this study due to a lack of data, thus the effects of O₃ on ISOP were not considered for PFTs other than deciduous broadleaf trees.

We eliminated the anomalously high values of deciduous broadleaf trees by generating a boxplot and performed a linear regression on the remaining data. The remaining data points in Fig. 1b show that RE is larger than 1 with AOT40 below 5 ppm h and smaller than 1 with AOT40 above 5 ppm h. This pattern suggested that low O₃ exposure can slightly stimulate ISOP emissions, while ISOP would be inhibited as O₃ accumulates. In general, there is a strong negative correlation between RE and AOT40 ($P < 0.01$), indicating that the ISOP emission rate of deciduous broadleaf trees would decline under long-term O₃ exposure. Compared to this work, another study Yuan et al. (2017) also suggested a negative response of ISOP emissions to O₃ exposure, with a larger declining rate (a slope of -0.02). The main reason is that only the most O₃-sensitive species, *Poplar*, was included in the regression model in that work.

The physiological and biochemical mechanisms of the effect of O₃ on ISOP have been investigated in a few studies. Yuan et al. (2016) assumed that the damage to photosynthesis from O₃ exposure would result in an increase in intercellular CO₂ and would elevate the consumption of phosphoenolpyruvate necessary for ISOP generation, leading to a reduced ISOP emission rate. Calfapietra et al. (2007) found that reduced ISOP emissions may result from the inhibition of the expression and activity of protein synthesis. Consistent with these findings, our regression suggested that ISOP emission decreased linearly with elevated O₃ exposure overall, despite a limited growth with increased O₃ exposure at a low AOT40 that may be caused by an oxygenated defense mechanism (Spinelli et al., 2011).

3.1.2. Reduced ISOP emissions due to O₃ exposure

Applying the Kriging interpolation function, we obtained the gridded O₃ concentration distribution across the YRD based on the observation data mentioned in Section 2.5. Fig. 2 in the supplement presents the time series of the diurnal average O₃ concentration and exposure dose (AOT40) across the YRD region during the growing season in 2015. The high O₃ concentrations over 40 ppb occurred mostly in May, June, and September but less often in July and August. AOT40 slowly increased as O₃ accumulated throughout the growing season, peaking at 14 ppm h at the end. The temporal variation in O₃ concentration resulted mainly from the changes in meteorology. The growth in O₃ concentration from April to June was attributed partly to the elevated temperature and solar radiation. Remarkably, the O₃ concentration slightly declined in the warmer months of July and August, and it could be related to the increased rainfall. Regarding the spatial distribution, as shown in Fig. S3 in the supplement, higher O₃ concentrations were found in the eastern YRD region and lower concentrations in the west, generally consistent with the spatial patterns of the industry and

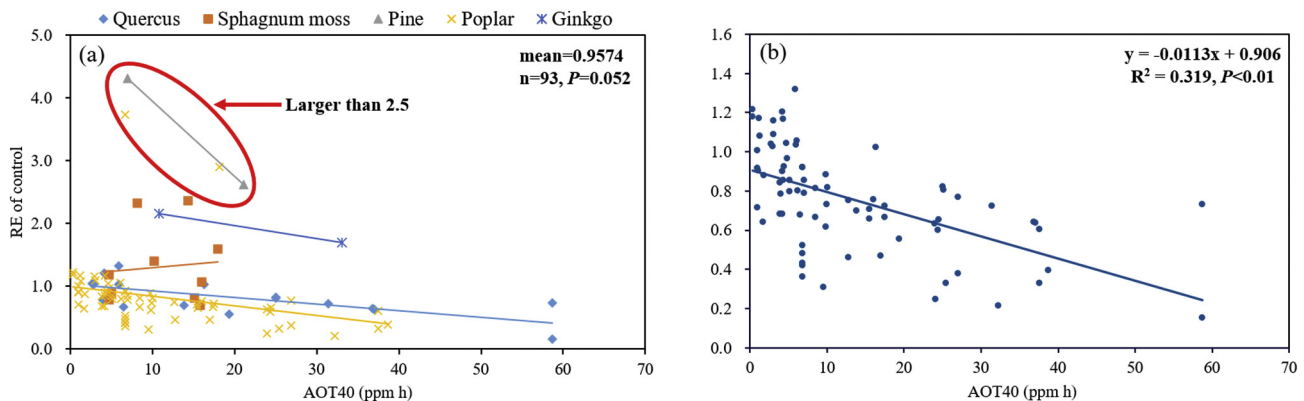


Fig. 1. The correlation between response values (RE) and AOT40 by species (a), and the linear relationship between RE and AOT40 in deciduous broadleaf tree (b). RE is reported as of control (treatment/control).

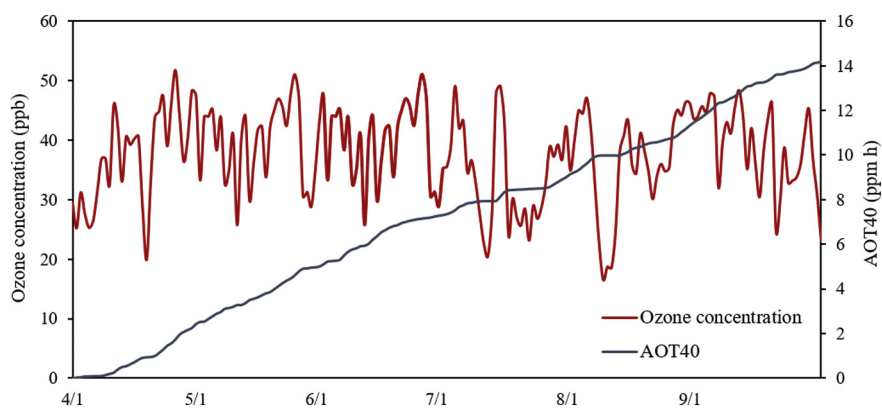


Fig. 2. Diurnal O₃ concentration and exposure dose (AOT40) during the growing season (April–September) in 2015 in the YRD region.

economy in the region. The O₃ concentrations were higher in the economically developed cities, including Shanghai, Nanjing, Hangzhou, Suzhou, Wuxi, and Ningbo, indicating that the urbanization and industrialization of the YRD city cluster played an important role on enhancement of the O₃ concentration. In the west YRD (particularly southern Anhui), the O₃ concentrations were relatively low because of the slower industrial development and limited emissions of O₃ precursors. In addition, the spatial pattern of O₃ varied by season. In spring (April and May), high-O₃ areas occurred across the eastern YRD region. These areas gradually shrank eastward in summer (June, July, and August) and then expanded again in autumn (September).

Table 2 summarizes the ISOP emissions by month and province in Case 1 and the relative changes in emissions in Case 2 that incorporated the O₃ exposure-response function and the actual AOT40 in the YRD region. The ISOP emissions in the YRD region were calculated at 8.6, 85.3, 341.7 and 82.6 Gg in January, April, July and October in Case 1, respectively. The O₃ exposure was estimated to reduce the ISOP emissions in the region by 1.0, 10.8 and 3.0 Gg in April, July and October in Case 2, accounting for 1.2%, 3.1% and 3.6% of the emissions without O₃ stress (Case 1), respectively. The accumulation of O₃ over time exaggerated the inhibition of the ISOP emissions. However, such inhibition slowed down as time went on because O₃ concentrations above 40 ppb occurred more frequently in spring than summer.

By comparing Cases 1 and 2, Fig. 3 illustrates the spatial patterns of the ISOP emission reduction due to O₃ exposure in different seasons. The O₃-ISOP effect in Case 2 mainly resulted in ISOP emission reduction in the central and northern YRD regions, with especially large impact on certain cities along the Yangtze River including Nanjing, Wuxi and Suzhou in Jiangsu Province, Chuzhou and Ma'anshan in Anhui Province, Huzhou and Jiaxing in Zhejiang Province, and Shanghai. The reduction rates of the ISOP emissions are summarized by city in Table S5 in the supplement and most of the reduction occurred in Jiangsu and Shanghai (Table 2). The largest reduction was found in Suzhou, with the ISOP emissions reduced by 10%, 25% and 39% in April, July and October,

respectively. The main influential factors of the ISOP emission reduction included the area fraction of deciduous broadleaf forest and O₃ exposure level. There was a relatively large fraction of the deciduous broadleaf forest area and high AOT40 in southern Jiangsu, and a significant reduction in ISOP emissions was estimated for the region in Case 2 compared to Case 1. Despite the more densely distributed deciduous broadleaf forests in western and southern Anhui Province, the reduction in ISOP emissions was relatively small, attributed mainly to the lower O₃ exposure level in these regions, as shown in Table 2. The O₃ exposure level was thus expected to have a greater impact on the ISOP emissions compared to the distribution of the deciduous broadleaf forest area across the YRD region.

3.2. Impact of the input data on BVOCs emissions

3.2.1. Discrepancies in the EFs and PFTs between various datasets

Combining the local emission measurements and the spatial distribution of plant species, we developed a set of local EFs of ISOP for the YRD region. Table 3 compares the EFs of ISOP applied in this study with global ones. In general, the local EFs are significantly smaller for needle trees, shrubs and grasslands and much larger for broadleaf trees and crop. The substantial discrepancies between the global and local EFs could result both from the various emission rates measured for specific plant species and the different species compositions for given PFT. For example, larger emission rate was measured for Chinese bamboos than the global average that hardly included the measurement from China (Li, 2015). Besides, abundant *Phyllostachys pubescens* forest (33% of broadleaf tree, as shown in Table S3) with relatively larger emission rate compared to other broadleaf tree species was found in the YRD region, elevating the EF for the PFT of broadleaf tree.

Regarding the land cover distribution, Fig. S4 in the supplement illustrates the area fractions of six land cover types in CCI, MULTI and MODIS. Similar spatial patterns with different densities for the forests were found in the YRD region among the three datasets. CCI had similar

Table 2
The ISOP emissions in Case 1 and the reduction rates of ISOP emissions due to O₃ exposure (i.e., (Case 1–Case 2)/Case 1 × 100%) by month and province in the YRD region. The area fractions of deciduous broadleaf tree and AOT40 are provided for reference.

	Deciduous broadleaf tree (%)	January ¹				April			July			October		
		ISOP (Gg)	ISOP (Gg)	AOT40 (ppm h)	Reduction rate (%)	ISOP (Gg)	AOT40 (ppm h)	Reduction rate (%)	ISOP (Gg)	AOT40 (ppm h)	Reduction rate (%)			
Jiangsu	2.1	0.1	1.8	1.1	9.8	9.6	14.2	19.8	1.8	21.3	27.2			
Shanghai	0.7	0.0	0.0	1.3	5.4	0.3	17.8	14.0	0.1	30.0	23.4			
Anhui	6.7	1.3	16.6	0.2	2.0	73.1	3.4	6.1	16.2	4.8	6.4			
Zhejiang	4.8	7.2	66.9	1.2	0.8	258.6	11.2	1.7	64.5	19.0	2.2			
YRD	4.7	8.6	85.3	0.8	1.2	341.7	9.0	3.2	82.6	14.2	3.6			

Note: there was no ISOP reduction in Case 2 for January, since January was within the growing season.

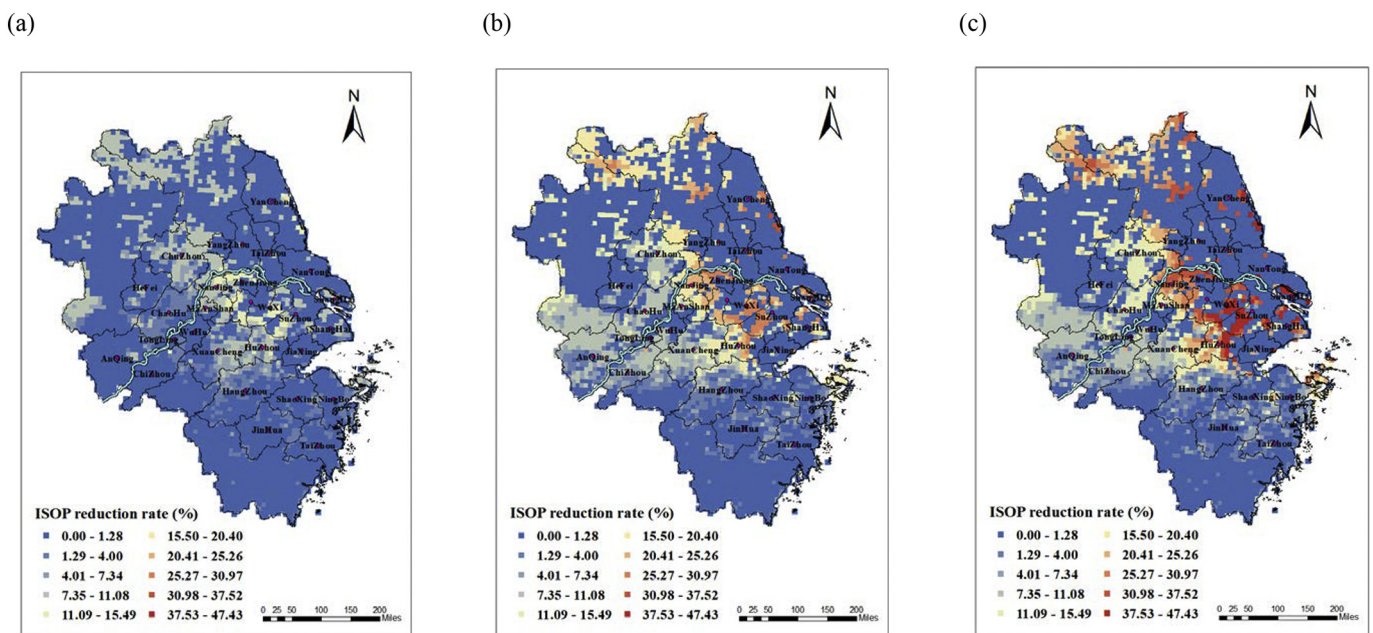


Fig. 3. The spatial distribution of ISOP reduction rate due to O₃ exposure (i.e., (Case 1- Case 2)/Case 1) in the YRD region in (a) April, (b) July, and (c) October 2015. The solid blue line represents the Yangtze River, and the red dots represent the city cluster along the Yangtze River.

fractions of broadleaf and needle trees, but the fraction of needle trees was larger than that of broadleaf trees in the southern YRD region. According to the forest resource survey of Zhejiang Province (Zhejiang Forestry Administration, <http://www.zjly.gov.cn/>), however, the broadleaf forest area exceeded that of needle forest in 2015. The result indicates that CCI may underestimate the broadleaf forest fraction (the main source of ISOP) in the YRD region, leading to underestimation of the ISOP emissions. In contrast, the fraction of broadleaf tree in MODIS was much larger than that of needle trees and was the largest among the three datasets. MODIS defined trees with a canopy higher than 2 m and a tree coverage larger than 10% as broadleaf trees. This criterion was looser than other land cover classifications that required tree coverage from 15% to 40% (Poulter et al., 2015), and it led to a larger fraction of broadleaf trees in MODIS. In contrast to the other two datasets, needle trees were concentrated in the central YRD in MODIS. The spatial distributions of shrubs and grasses vary among the three datasets as well. However, their influence on ISOP emission estimation may be limited due to their relatively low ISOP emission rates and small area fractions. Compared to MULTI, the cropland fractions were larger and the city and countryside land fractions were smaller in the two satellite datasets. The overestimation of croplands in the satellite products resulted possibly from the high mixing of croplands with other land use types, and complicated land cover features could not be fully captured by satellites due to sensor detection limit.

The area fractions of the land use types in the three land datasets are summarized in Table 3, and the discrepancies in the distribution of broadleaf trees (8%–30%) and croplands (32%–61%) were more

Table 3
The global and local ISOP emission factors ($\mu\text{g m}^{-2} \text{h}^{-1}$) and the area fractions in the three land cover datasets across the YRD region by land cover type.

	EF		Land cover		
	Guenther et al. (Global)	This study (YRD)	CCI	MULTI	MODIS
Needleleaf tree	600	27	9.7%	4.0%	8.4%
Broadleaf tree	10,000	16,619	8.3%	22.6%	30.3%
Shrub	4000	1180	5.2%	2.8%	0.0%
Grass	800	70	6.0%	3.1%	2.0%
Crop	1	40	60.5%	51.6%	32.2%

significant. The fraction of broadleaf forests was the largest in MODIS and the smallest in CCI, while the opposite pattern was found for croplands. The discrepancy in the distribution of broadleaf trees with high emission rates could have a greater impact on ISOP emission estimation, while the influence of croplands with low ISOP emission rates could be relatively weak. The proportion of needle trees in MULTI is smaller than those in CCI and MODIS. Shrubs and grasslands both had similar and relatively small fractions in the three datasets.

3.2.2. Sensitivity of the BVOCs emissions to the EFs and land cover

Table 4 summarizes the simulated emissions of BVOCs and ISOP and the relative changes in Cases 3–5 to Case 1 for July 2015. The BVOCs and ISOP emissions for July were estimated at 584 and 342 Gg, respectively, across the YRD region in Case 1. As shown in Fig. 4a, most of ISOP emissions were concentrated in the southern YRD region and the mountain areas in western Anhui due to the abundant forests, intense sunlight and high temperatures. The estimated BVOCs and ISOP emissions with global EFs (Case 3) were 21% and 37% smaller than those with local EFs (Case 1) respectively. As the YRD is covered mostly by broadleaf trees and crops with local EFs that are larger than the global ones (Table 3), the ISOP emissions declined all over the YRD region when applying global EFs, especially in the southern YRD (Fig. 4b). However, in certain northern regions dominated by shrubs, grasses and needle trees, elevated emissions were observed with larger EFs in global level in Case 3. The discrepancies in EFs not only led to various estimates of the total BVOCs emissions but also significantly changed the mass fractions of the chemical species in the emissions. Fig. S5 in the supplement shows that the fraction of ISOP was greatly reduced from 59% to 47% in

Table 4
The estimation of BVOCs and ISOP emissions in different cases across the YRD region in July 2015.

	Case 1	Case 3	Case 4	Case 5
BVOCs (Gg)	583.6	458.5	384.0	868.9
ISOP (Gg)	341.7	216.5	131.5	567.0
BVOCs _{relative}	–	78.6%	65.8%	148.9%
ISOP _{relative}	–	63.4%	38.5%	166.0%

Note: BVOCs_{relative} and ISOP_{relative} mean the ratios of BVOCs and ISOP emissions in Cases 3, 4, and 5 relative to Case 1, respectively.

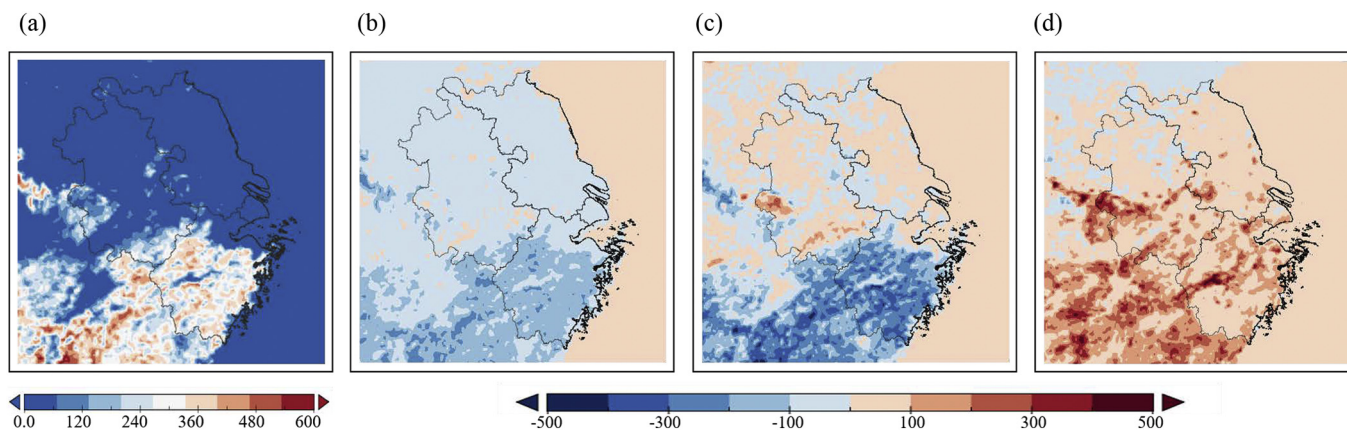


Fig. 4. The spatial distribution of (a) ISOP emissions in Case 1, and emission differences between (b) Cases 3 and 1, (c) Cases 4 and 1, and (d) Case 5 and 1 in July 2015.

Case 3, attributed to the global EFs of the ISOP source (e.g., broadleaf trees) that are smaller than the local ones.

Compared to the EFs, the vegetation distribution had a greater impact on the quantification and spatial distribution of the ISOP emissions. According to Cases 4 and 5, the results based on CCI may underestimate the ISOP emissions by 61%, while those based on MODIS may overestimate the emissions by 66% in the YRD (Table 4). Attributed to the various monitoring methods and classification systems, the fractions of certain PFTs were significantly different among the three datasets, particularly for broadleaf forests and crop (Fig. S4 and Table 3), and the discrepancy in broadleaf forest distribution would influence ISOP emission estimation more notably due to its larger EFs compared to the other PFTs. As a result of the smaller area fraction of broadleaf tree in CCI compared to those in MULTI, application of CCI underestimated the ISOP emissions mainly in the southern YRD but overestimated the emissions in certain forest areas in Anhui Province (Fig. 4c). In contrast, application of MODIS overestimated the ISOP emissions in most of the YRD region (Fig. 4d), as the distribution of broadleaf tree in MODIS was relatively extensive. In the northern YRD, adopting MODIS data underestimated the ISOP emissions, as there were few broadleaf trees

in MODIS but some in MULTI. Compared to the broadleaf tree, the difference in crop distribution had less influence on ISOP emission estimation due to its smaller EF. Smaller differences were found for the emission estimations of MON and SQT with the three datasets. Compared to MULTI, application of CCI underestimated MON and SQT by 8% and 11%, while MODIS overestimated them by 66% and 61%, respectively. As illustrated in Fig. S6a in the supplement, the underestimation of MON by CCI occurred mainly in central YRD where less needle trees with relatively large MON EFs were suggested by CCI than MULTI. Similarly, the overestimation of MON by MODIS occurred in areas with more needle trees than MULTI, especially in southern Anhui and western Jiangsu (Fig. S6d). The changes in SQT emissions were fewer (Fig. S6b and e), due to the smaller EF for each PFT. For other VOCs species, the estimations of CCI and MODIS were respectively 7% and 16% larger than that of MULTI (Fig. S6c and f), attributed mainly to the overestimation of crop in northern YRD. The various land cover data led to discrepancy in the speciation of the BVOCs emissions, especially for ISOP, as shown in Fig. S7 in the supplement. Similar to that of the broadleaf trees, the fraction of ISOP to total BVOCs was the largest in MODIS (65%) and the smallest in CCI (34%). The fractions of MON and SQT did not change

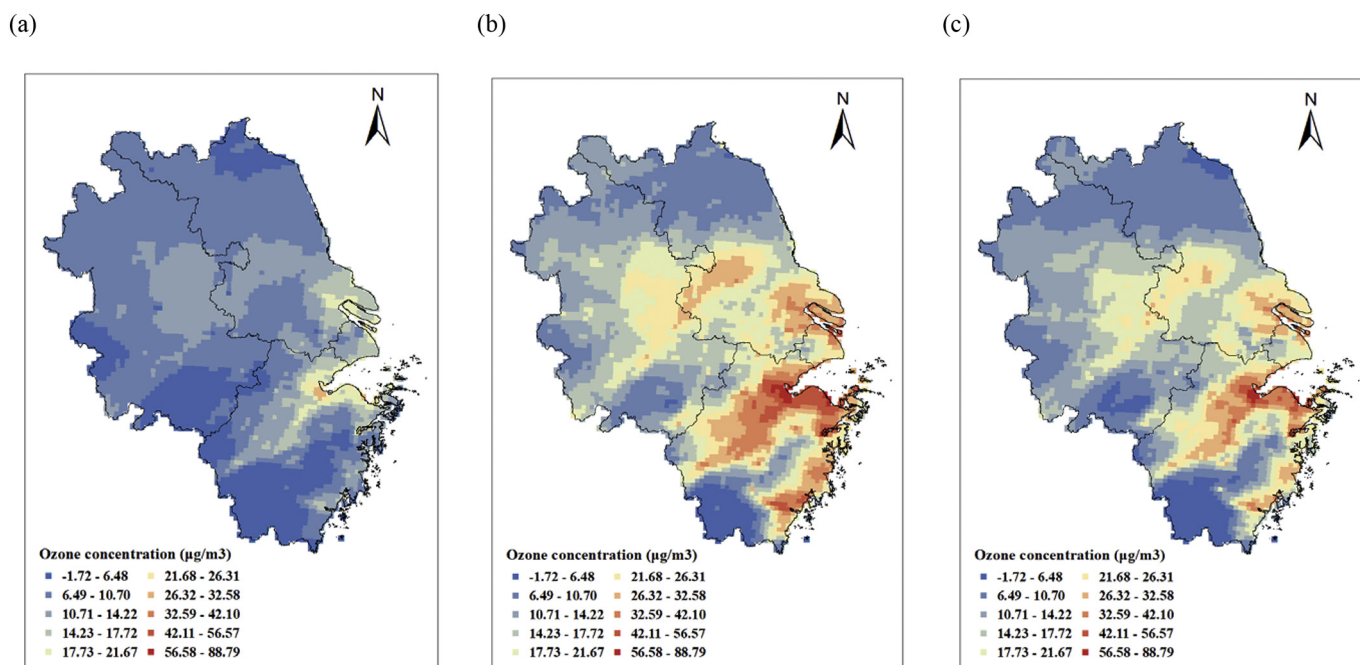


Fig. 5. The contribution of BVOCs to (a) 1h_average, (b) MDA1 and (c) MDA8 in July 2015 across the YRD region.

significantly due to their relatively small emission amount, while that of other VOCs presented an opposite pattern to ISOP, i.e., the largest in CCI (55%) and smallest in MODIS (26%).

3.3. Impact of the BVOCs on the O₃ simulations

3.3.1. The contributions of BVOCs to O₃ formation

As illustrated in Fig. S8 in the supplement, the total BVOCs emissions for January, April, July and October 2015 were calculated at 909.3 Gg in Case 2 for the YRD region, while the corresponding AVOC emissions were estimated at 2190.8 Gg in MEIC. The BVOCs emissions were abundant in the southern YRD such as Zhejiang due to the dense forests and favorable climates in the area, while larger AVOCs emissions were found in Jiangsu with the intensive refineries and chemical engineering industries (Zhao et al., 2017). Affected by meteorological factors and leaf physiological conditions, the BVOCs presented seasonal variations with the highest emissions in July (63%), followed by those in April (18%) and October (17%) and the lowest in January (2%).

As described in Section 2.6, the difference in simulated O₃ concentrations between Cases 2 and 6 represented the contribution of BVOCs to O₃ formation. Fig. 5 illustrates the spatial patterns of the BVOCs contributions to the monthly average values of 1 h mean (1h_average), the maximum daily 1-h (MDA1), and the maximum daily 8-h (MDA8) O₃ concentration. The areas with high BVOCs contributions were found in eastern and north-central YRD, and these areas did not agree well with the areas with high BVOCs emissions, e.g., the southern YRD region, as shown in Fig. S9a in the Supplement. With a strong chemical reactivity, BVOCs usually react shortly after they are released, thus their effect on O₃ formation would depend more on local sources. In addition, the spatial difference in the contributions of BVOCs to O₃ formation could be closely related to precursor emissions and relative levels of the non-methane hydrocarbons to NO_x in the atmosphere in various regions. By comparing the spatial distributions of the BVOCs contributions (Fig. 5) and NO_x emissions (Fig. S9b), we found that the areas with large BVOCs contributions to O₃ formation were close to those with abundant NO_x emissions. Pearson correlation analysis suggested that the two sets of data were significantly correlated in the spatial distribution ($P < 0.001$), indicating that the BVOCs contribution to O₃ formation was restricted by NO_x emissions rather than BVOCs themselves. Jin and Holloway (2015) indicated that the eastern and north-central YRD were mostly VOC-limited or mixed areas for O₃ formation, i.e., the O₃ generation was more sensitive to VOCs (including BVOCs). Therefore, controlling the BVOCs emissions in areas with abundant NO_x emission would be helpful in mitigating O₃ pollution. In contrast, the BVOCs emissions in certain forestlands reduced O₃ formation in

southern Zhejiang. This might be because there were limited NO_x emissions in the region, and a large amount of ISOP emissions were oxidized through the considerable consumption of O₃.

Across the YRD region, BVOCs contributed more to MDA1 (12%) and MDA8 (11%), but less to 1h_average (10%). The difference in BVOCs contributions to the three O₃ indices could be partly due to the combined effects of the varied diurnal meteorological conditions and pollutant emission levels. Fig. 6 shows the diurnal variations in the BVOCs contributions in the different provinces and the NO_x emission rates across the YRD. The NO_x emissions were distributed in a pattern with two peaks at 9:00 AM and 7:00 PM and both peaks were caused by the large amount of vehicles during the daily traffic rush hours. The contributions of BVOCs to O₃ formation increased rapidly from 6:00 AM, reached a peak at noon (10:00 AM–3:00 PM) and decreased rapidly at dusk (6:00 PM). With the elevated solar radiation, NO_x was strongly involved in photochemical reactions with atmospheric oxidants and decreased in the afternoon. In contrast, the BVOCs emissions would be elevated with increased light and temperatures. After 6:00 AM, the BVOCs emissions increased and reacted with NO_x to gradually form O₃. In general, a large contribution of BVOCs was found for all regions at noon with high O₃ concentrations, thus BVOCs would contribute more to the extremely high concentrations (MDA1 and MDA8) than the average (1h_average).

The bias in the estimation of BVOC contribution to O₃ formation should be noted. As the O₃ formation is a strong nonlinear process, removing one source to determine its contribution (the so-called Brute-force method) resulted in potentially high uncertainty. The results should thus be interpreted cautiously. This work implied that BVOCs had a significant impact on the spatial and temporal distributions of O₃ formation. O₃ pollution episodes with extremely high concentrations were likely to occur in regions with abundant NO_x emissions. Therefore, BVOCs emission abatement needs to be considered in those regions to reduce the risk of O₃ formation on human health and the ecosystem. For example, tree species adjustment could be a feasible way to mitigate BVOCs emissions. Changing a certain fraction of species with large ISOP EFs such as *Poplar* and *Quercus* to the combination of low-emitting species like *Castanopsis* and *Salix* was expected to be helpful for limiting the ISOP fluxes (Ren et al., 2017).

3.3.2. Sensitivity of the O₃ simulations to the BVOCs emissions

The spatial distribution of difference in simulated O₃ concentrations between Cases 1 and 2 in July 2015 is shown in Fig. S10 in the supplement. Compared to Case 2, ISOP inhibition caused by the actual O₃ exposure in Case 1 resulted in slight reduction in O₃ simulation (−1.9%–+0.07% by grid) across the YRD region. The spatial pattern of O₃

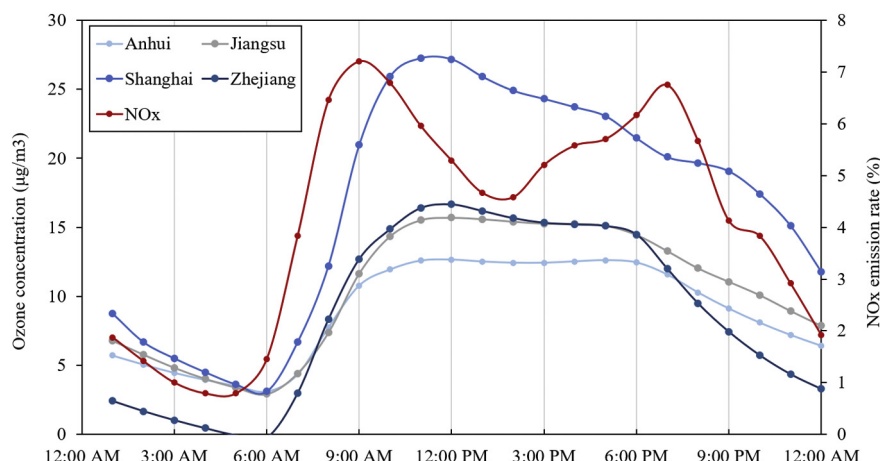


Fig. 6. Diurnal variations of BVOCs contribution to O₃ formation ($\mu\text{g}/\text{m}^3$) by province and that of NO_x emissions (%) in the YRD region in July 2015.

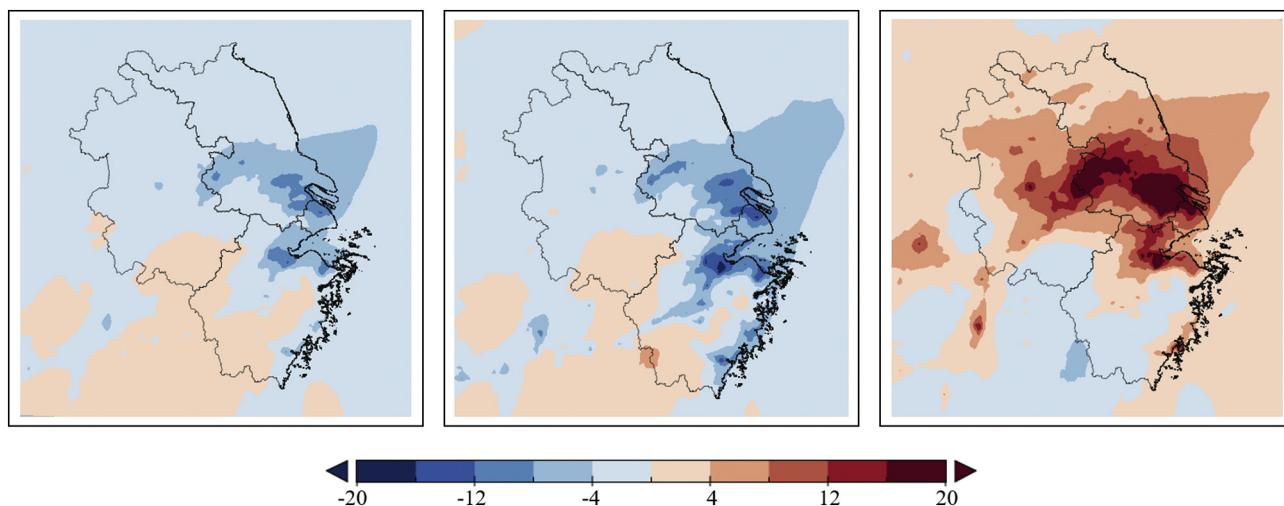


Fig. 7. The spatial distribution of difference of O₃ concentrations (1h_average) between (a) Cases 3 and 1, (b) Cases 4 and 1, and (c) Cases 5 and 1 in July 2015 (unit: %).

reduction was similar to that of ISOP reduction (Fig. 3b), i.e., more significant in the central and northern YRD regions where ISOP contributed more to O₃ (Fig. 5a). In recent years, O₃ production have increased in urban areas of YRD region significantly because of the increased VOC emissions, decreased NO_x emissions and reduced ambient PM_{2.5} levels. However, the O₃ enhancement caused by anthropogenic activities might be partly weakened through the restrained biogenic ISOP emissions by O₃ exposure.

Fig. 7 illustrates the spatial patterns of the differences in the simulated O₃ concentrations relative to the Case 1 for Cases 3–5 for July 2015. By comparing Case 1 and 3, the discrepancy between the global and local EFs eventually led to a difference in the O₃ simulation results of 3% (−12.7%~+3.9% by grid) across the YRD region. A larger reduction in O₃ concentrations was found in the eastern and central YRD, especially in Shanghai at 6% (Fig. 7a). Although the BVOCs emissions decreased more with global EFs in the southern YRD (Fig. 3b), the O₃ changes due to EFs were mainly found in the eastern and north-central YRD, consistent with the distribution of the BVOCs contributions to O₃ formation (Fig. 5). This is mainly because the contribution of BVOCs to O₃ formation was more related to NO_x emissions than to the BVOCs themselves, as discussed in Section 3.3.1. Therefore, the large BVOCs reduction in the southern YRD did not cause dramatic changes in O₃ formation, while a relatively small reduction in the eastern YRD would lead to stronger O₃ changes. The reduction in BVOCs in the southwestern areas resulted in slightly enhanced O₃ levels, possibly because a large amount of the ISOP emissions was consumed to deplete O₃.

Similar spatial distributions were found for the impacts of different land cover inputs on O₃ simulations, as shown in Fig. 7b and c. Across the whole YRD region, the 1h_averages of CCI and MODIS differed by 3% and 5%, respectively, from that of MULTI. The spatial distributions of the differences were also consistent with those of the BVOCs contributions to O₃ formation, which was mainly in the plains of the lower reaches of the Yangtze River. The ISOP underestimation by CCI in the eastern YRD led to decreased O₃, while the overestimation by MODIS in the central and east regions led to increased O₃. Compared to CCI, the difference in simulated O₃ concentrations caused by MODIS was more significant because the application of MODIS data resulted in a greater extent and a wider range of overestimation in the ISOP emissions. Fig. S11 in the supplement shows the hourly averaged O₃ concentrations from observation and simulations with the above three cases, as well as Case 6 in which BVOCs were removed. Overestimation can be found for all the cases including Case 6 without BVOCs emissions. As most of the YRD region was VOC-limited for O₃ formation, revising the BVOC emissions alone could not improve the model performance. Further efforts were thus recommended to identify the crucial factors on

O₃ simulation (e.g., the NO_x and AVOCs emissions and meteorology) and to improve the model performance.

4. Conclusions

To examine the effect of O₃ stress on ISOP emissions, we developed an O₃ exposure–ISOP response function through meta-analysis. Incorporating the O₃–ISOP effect for deciduous broadleaf tree into MEGAN, the ISOP emissions were calculated during the growing season of 2015 across the YRD region. Different EF databases and land cover datasets were developed and adopted to investigate the sensitivities of the simulated BVOCs emissions and O₃ concentrations to the input variables. We found that the ISOP emissions would be restrained with increased O₃ exposure in the central and lower plains of the Yangtze River during the growing season, and a maximum reduction was found for the city of Suzhou. The application of global default EFs led to a 47% underestimation in the ISOP emissions, and the land cover inputs, with various locations and amounts of broadleaf trees, had a larger impact on the emission estimation and spatial distribution of ISOP. Affected by the anthropogenic NO_x, a greater contribution to O₃ formation was found for BVOCs in the eastern and north-central YRD compared to the south, and the slight change in BVOCs emission with different input variables resulted in considerable variation in O₃ simulation. In contrast, there was limited change in O₃ simulation in the southern YRD even with noticeable difference in the BVOC emissions. Additionally, due to the diurnal variations in emissions and meteorology, the BVOCs contributed more to the extremely high O₃ concentrations than the average. Therefore, the BVOC emissions should be better considered in future air quality prediction studies.

This study considers the O₃–ISOP effect for deciduous broadleaf trees in BVOC estimations across the YRD region. Due to insufficient results from O₃–plant fumigation experiments, however, we could not quantify the feedback effects for other plant types and VOC species other than ISOP. More O₃ fumigation experiments are recommended for further improvement of the exposure–response function. In addition, uncertainty existed in the O₃ exposure estimation with the Kriging interpolation, due mainly to the limited coverage of ground monitoring sites. Multi-source data fusion, including air quality modeling, satellite retrievals and ground observations, is suggested to improve O₃ exposure estimation and thereby BVOC emission estimation in the future.

CRedit authorship contribution statement

Yutong Wang: Methodology, Investigation, Data curation, Software, Writing - original draft. **Yu Zhao:** Conceptualization, Methodology,

Resources, Writing - review & editing. **Lei Zhang:** Resources, Data curation. **Jie Zhang:** Resources, Data curation. **Yang Liu:** Writing - review & editing.

Declaration of competing interest

The authors declare that they have no known competing financial interests or personal relationships that could have appeared to influence the work reported in this paper.

Acknowledgement

This work was sponsored by the National Key Research and Development Program of China (2017YFC0210106) and the Natural Science Foundation of China (41922052 and 91644220). Vegetation Atlas of China (1:1,000,000) was supported by the 13th Five-year Informatization Plan of Chinese Academy of Sciences, Grant No. XXH13505-07. We would like to acknowledge Tong Dan from Tsinghua University for the national emission data (MEIC), and Xiangyang Yuan from Research Center for Eco-environmental Sciences, Chinese Academy of Sciences for helpful comments on the effect of O₃ on plants.

Appendix A. Supplementary data

Supplementary data to this article can be found online at <https://doi.org/10.1016/j.scitotenv.2020.138703>.

References

- Arneeth, A., Niinemets, U., Pressley, S., Back, J., Hari, P., Karl, T., Noe, S., Prentice, I.C., Serca, D., Hickler, T., Wolf, A., Smith, B., 2007. Process-based estimates of terrestrial ecosystem isoprene emissions: incorporating the effects of a direct CO₂-isoprene interaction. *Atmos. Chem. Phys.* 7, 31–53.
- Calafapietra, C., Wiberley, A.E., Falbel, T.G., Linskey, A.R., Mugnoz, G.S., Karnosky, D.F., Loreto, F., Sharkey, T.D., 2007. Isoprene synthase expression and protein levels are reduced under elevated O₃ but not under elevated CO₂ (FACE) in field-grown aspen trees. *Plant Cell and Environ.* 30, 654–661.
- Chen, W.H., Guenther, A.B., Wang, X.M., Chen, Y.H., Gu, D.S., Chang, M., Zhou, S.Z., Wu, L.L., Zhang, Y.Q., 2018. Regional to global biogenic isoprene emission responses to changes in vegetation from 2000 to 2015. *J. Geophys. Res.-Atmos.* 123, 3757–3771.
- Chen, C., Park, T., Wang, X., Piao, S., Xu, B., Chaturvedi, R.K., Fuchs, R., Brovkin, V., Ciais, P., Fensholt, R., Tommervik, H., Bala, G., Zhu, Z., Nemani, R.R., Myneni, R.B., 2019. China and India lead in greening of the world through land-use management. *Nat. Sustain.* 2, 122–129.
- Emery, C., Tai, E., Yarwood, G., 2001. Enhanced Meteorological Modeling and Performance Evaluation for Two Texas Episodes, Report to the Texas Natural Resources Conservation Commission, Prepared by ENVIRON. International Corp, Novato, CA.
- Feng, Z., Yuan, X., 2018. Effects of elevated ozone on biogenic volatile organic compounds (BVOCs) emission: a review. *Environ. Sci.* 39, 5257–5265.
- Fu, Y., Liao, H., 2012. Simulation of the interannual variations of biogenic emissions of volatile organic compounds in China: impacts on tropospheric ozone and secondary organic aerosol. *Atmos. Environ.* 59, 170–185.
- Fu, Y., Liao, H., 2014. Impacts of land use and land cover changes on biogenic emissions of volatile organic compounds in China from the late 1980s to the mid-2000s: implications for tropospheric ozone and secondary organic aerosol. *Tellus B* 66, 24987.
- Fu, Y., Tai, A.P.K., 2015. Impact of climate and land cover changes on tropospheric ozone air quality and public health in East Asia between 1980 and 2010. *Atmos. Chem. Phys.* 15, 10093–10106.
- Fu, T.M., Jacob, D.J., Palmer, P.I., Chance, K., Wang, Y.X., Barletta, B., Blake, D.R., Stanton, J.C., Pilling, M.J., 2007. Space-based formaldehyde measurements as constraints on volatile organic compound emissions in east and south Asia and implications for ozone. *J. Geophys. Res.-Atmos.* 112.
- Fu, X., Wang, S.X., Zhao, B., Xing, J., Cheng, Z., Liu, H., Hao, J.M., 2013. Emission inventory of primary pollutants and chemical speciation in 2010 for the Yangtze River Delta region, China. *Atmos. Environ.* 70, 39–50.
- Geng, F., Tie, X., Guenther, A., Li, G., Cao, J., Harley, P., 2011. Effect of isoprene emissions from major forests on ozone formation in the city of Shanghai, China. *Atmos. Chem. Phys.* 11, 10449–10459.
- Gong, D., Wang, H., Zhang, S., Wang, Y., Liu, S.C., Guo, H., Shao, M., He, C., Chen, D., He, L., Zhou, L., Morawska, L., Zhang, Y., Wang, B., 2018. Low-level summertime isoprene observed at a forested mountaintop site in southern China: implications for strong regional atmospheric oxidative capacity. *Atmos. Chem. Phys.* 18, 14417–14432.
- Guenther, A.B., Hewitt, C.N., Erickson, D., Fall, R., Geron, C., Graedel, T., Harley, P., Klinger, L., Lerdau, M., McKay, W.A., Pierce, T., Scholes, B., Steinbrecher, R., Tallamraju, R., Taylor, J., Zimmerman, P., 1995. A global model of natural volatile organic compound emissions. *J. Geophys. Res.-Atmos.* 100, 8873–8892.
- Guenther, A.B., Jiang, X., Heald, C.L., Sakulyanontvittaya, T., Duhl, T., Emmons, L.K., Wang, X., 2012. The Model of Emissions of Gases and Aerosols from Nature version 2.1 (MEGAN2.1): an extended and updated framework for modeling biogenic emissions. *Geosci. Model Dev.* 5, 1471–1492.
- Jin, X.M., Holloway, T., 2015. Spatial and temporal variability of ozone sensitivity over China observed from the Ozone Monitoring Instrument. *J. Geophys. Res.-Atmos.* 120, 7229–7246.
- Laothawornkitkul, J., Taylor, J.E., Paul, N.D., Hewitt, C.N., 2009. Biogenic volatile organic compounds in the Earth system. *New Phytol* 183, 27–51.
- Li, L.Y., 2015. Characteristics of Biogenic VOCs Emission and Its High-resolution Emission Inventory in China. Ph. D thesis. Peking University, Beijing, China.
- Li, L.Y., Chen, Y., Xie, S.D., 2013. Spatio-temporal variation of biogenic volatile organic compounds emissions in China. *Environ. Pollut.* 182, 157–168.
- Li, L., An, J.Y., Shi, Y.Y., Zhou, M., Yan, R.S., Huang, C., Wang, H.L., Lou, S.R., Wang, Q., Lu, Q., Wu, J., 2016. Source apportionment of surface ozone in the Yangtze River Delta, China in the summer of 2013. *Atmos. Environ.* 144, 194–207.
- Li, K., Jacob, D.J., Liao, H., Shen, L., Zhang, Q., Bates, K.H., 2019. Anthropogenic drivers of 2013–2017 trends in summer surface ozone in China. *Proc. Natl. Acad. Sci. U.S.A.* 116, 422–427.
- Li, M., Zhang, Q., Streets, D.G., He, K.B., Cheng, Y.F., Emmons, L.K., Huo, H., Kang, S.C., Lu, Z., Shao, M., Su, H., Yu, X., Zhang, Y., 2014. Mapping Asian anthropogenic emissions of nonmethane volatile organic compounds to multiple chemical mechanisms. *Atmos. Chem. Phys.* 14, 5617–5638.
- Liu, F., Zhang, Q., Tong, D., Zheng, B., Li, M., Huo, H., He, K., 2015. High-resolution inventory of technologies, activities, and emissions of coal-fired power plants in China from 1990 to 2010. *Atmos. Chem. Phys.* 15, 13299–13317.
- Liu, Y., Li, L., An, J., Huang, L., Yan, R., Huang, C., Wang, H., Wang, Q., Wang, M., Zhang, W., 2018. Estimation of biogenic VOC emissions and its impact on ozone formation over the Yangtze River Delta region, China. *Atmos. Environ.* 186, 113–128.
- Lou, S., Zhu, B., Liao, H., 2010. Impacts of O₃ precursor on surface O₃ concentration over China. *Trans. Atmos. Sci.* 33, 451–459.
- Marais, E.A., Jacob, D.J., Kurosu, T.P., Chance, K., Murphy, J.G., Reeves, C., Mills, G., Casadio, S., Millet, D.B., Barkley, M.P., Paulot, F., Mao, J., 2012. Isoprene emissions in Africa inferred from OMI observations of formaldehyde columns. *Atmos. Chem. Phys.* 12, 6219–6235.
- Niinemets, U., Tenhunen, J.D., Harley, P.C., Steinbrecher, R., 1999. A model of isoprene emission based on energetic requirements for isoprene synthesis and leaf photosynthetic properties for Liquidambar and Quercus. *Plant Cell Environ.* 22, 1319–1335.
- Ning, J., Liu, J., Kuang, W., Xu, X., Zhang, S., Yan, C., Li, R., Wu, S., Hu, Y., Du, G., Chi, W., Pan, T., Ning, J., 2018. Spatiotemporal patterns and characteristics of land-use change in China during 2010–2015. *J. Geophys. Res.* 28, 547–562.
- Paasonen, P., Asmi, A., Petaja, T., Kajos, M.K., Aijala, M., Junninen, H., Holst, T., Abbatt, J.P.D., Arneeth, A., Birmili, W., van der Gon, H.D., Hamed, A., Hoffer, A., Laakso, L., Laaksonen, A., Leaitch, W.R., Plass-Duelmer, C., Pryor, S.C., Rissanen, P., Swietlicki, E., Wiedensohler, A., Worsnop, D.R., Kerminen, V.-M., Kulmala, M., 2013. Warming-induced increase in aerosol number concentration likely to moderate climate change. *Nat. Geosci.* 6, 438–442.
- Penuelas, J., Staudt, M., 2010. BVOCs and global change. *Trends Plant Sci* 15, 133–144.
- Poulter, B., MacBean, N., Hartley, A., Khlstova, I., Arino, O., Betts, R., Bontemps, S., Boettcher, M., Brockmann, C., Defourny, P., Hagemann, S., Herold, M., Kirches, G., Lamarche, C., Lederer, D., Otle, C., Peters, M., Peylin, P., 2015. Plant functional type classification for earth system models: results from the European Space Agency's Land Cover Climate Change Initiative. *Geosci. Model Dev.* 8, 2315–2328.
- Price, C., Penner, J., Prather, M., 1997. NOx from lightning, part I: global distribution based on lightning physics. *J. Geophys. Res.* Atmos. 102.
- Ren, Y., Qu, Z., Du, Y., Xu, R., Ma, D., Yang, G., Shi, Y., Fan, X., Tani, A., Guo, P., Ge, Y., Chang, J., 2017. Air quality and health effects of biogenic volatile organic compounds emissions from urban green spaces and the mitigation strategies. *Environ. Pollut.* 230, 849–861.
- Shilling, J.E., Zaveri, R.A., Fast, J.D., Kleinman, L., Alexander, M.L., Canagaratna, M.R., Fortner, E., Hubbe, J.M., Jayne, J.T., Sedlacek, A., Setyan, A., Springston, S., Worsnop, D.R., Zhang, Q., 2013. Enhanced SOA formation from mixed anthropogenic and biogenic emissions during the CARES campaign. *Atmos. Chem. Phys.* 13, 2091–2113.
- Shim, C., Wang, Y.H., Choi, Y., Palmer, P.I., Abbot, D.S., Chance, K., 2005. Constraining global isoprene emissions with Global Ozone Monitoring Experiment (GOME) formaldehyde column measurements. *J. Geophys. Res.-Atmos.* 110.
- Sindelarova, K., Granier, C., Bouarar, I., Guenther, A., Tilmes, S., Stavrou, T., Muller, J.F., Kuhn, U., Stefani, P., Knorr, W., 2014. Global data set of biogenic VOC emissions calculated by the MEGAN model over the last 30 years. *Atmos. Chem. Phys.* 14, 9317–9341.
- Skamarock, W., Klemp, J., Dudhia, J., Gill, D., Barker, D., Duda, M., Huang, X., Wang, W., Powers, J., 2008. A Description of the Advanced Research WRF Version 3. NCAR Tech. Note NCAR/TN-475+STR, p. 113.
- Song, Y., 2012. Research on BVOCs Emission Characteristics in China Based on Remote Sensing. Nanjing university.
- Spinelli, F., Cellini, A., Marchetti, L., Mudigere, K., Piovone, C., 2011. Emission and Function of Volatile Organic Compounds in Response to Abiotic Stress. *Abiotic Stress in Plants - Mechanisms and Adaptations.* 16 pp. 367–394.
- Stavrakou, T., Muller, J.F., Bauwens, M., De Smedt, I., Van Roozendael, M., Guenther, A., Wild, M., Xia, X., 2014. Isoprene emissions over Asia 1979–2012: impact of climate and land-use changes. *Atmos. Chem. Phys.* 14, 4587–4605.
- Tiwari, S., Grote, R., Churkina, G., Butler, T., 2016. Ozone damage, detoxification and the role of isoprenoids - new impetus for integrated models. *Funct. Plant Biol.* 43, 324–336.
- Unger, N., 2014. Human land-use-driven reduction of forest volatiles cools global climate. *Nat. Clim. Change.* 4, 907–910.

- Velikova, V., Tsonev, T., Pinelli, P., Alessio, G.A., Loreto, F., 2005. Localized ozone fumigation system for studying ozone effects on photosynthesis, respiration, electron transport rate and isoprene emission in field-grown Mediterranean oak species. *Tree Physiology* 25, 1523–1532.
- von Kuhlmann, R., Lawrence, M.G., Poschl, U., Crutzen, P.J., 2004. Sensitivities in global scale modeling of isoprene. *Atmos. Chem. Phys.* 4, 1–17.
- Wang, X., Situ, S., Chen, W., Zheng, J., Guenther, A., Fan, Q., Chang, M., 2016. Numerical model to quantify biogenic volatile organic compound emissions: The Pearl River Delta region as a case study. *J. Environ. Sci.* 46, 72–82.
- Wang, T., Xue, L., Brimblecombe, P., Lam, Y.F., Li, L., Zhang, L., 2017. Ozone pollution in China: A review of concentrations, meteorological influences, chemical precursors, and effects. *Sci. Total Environ.* 575, 1582–1596.
- Wang, H., Wu, Q., Liu, H., Wang, Y., Cheng, H., Wang, R., Wang, L., Xiao, H., Yang, X., 2018. Sensitivity of biogenic volatile organic compound emissions to leaf area index and land cover in Beijing. *Atmos. Chem. Phys.* 18, 9583–9596.
- Warneke, C., Luxembourg, S.L., de Gouw, J.A., Rinne, H.J.J., Guenther, A.B., Fall, R., 2002. Disjunct eddy covariance measurements of oxygenated volatile organic compounds fluxes from an alfalfa field before and after cutting. *J. Geophys. Res.-Atmos.* 107, 4067.
- Wu, W., Yang, P., Zhang, L., Tang, H., Zhou, Q., Shibasaki, R., 2009. Accuracy assessment of four global land cover datasets in China. *Transactions of the CSAE* 25, 167–173.
- Wyat Appel, K., Napelenok, S.L., Foley, K.M., 2017. Description and evaluation of the community multiscale air quality (cmaq) modeling system version 5.1. *Geosci. Model Dev.* 10, 1–41.
- Xie, M., Wang, T., Jiang, F., Yang, X., 2007. Modeling of natural NO_x and VOC emissions and their effects on tropospheric photochemistry in China. *Environ. Sci.* 28, 32–40.
- Yuan, X., Calatayud, V., Gao, F., Fares, S., Paoletti, E., Tian, Y., Feng, Z., 2016. Interaction of drought and ozone exposure on isoprene emission from extensively cultivated poplar. *Plant Cell and Environ.* 39, 2276–2287.
- Yuan, X., Feng, Z., Liu, S., Shang, B., Li, P., Xu, Y., Paoletti, E., 2017. Concentration-and flux-based dose-responses of isoprene emission from poplar leaves and plants exposed to an ozone concentration gradient. *Plant Cell and Environ.* 40, 1960–1971.
- Zhao, Y., Mao, P., Zhou, Y., Yang, Y., Zhang, J., Wang, S., Dong, Y., Xie, F., Yu, Y., Li, W., 2017. Improved provincial emission inventory and speciation profiles of anthropogenic non-methane volatile organic compounds: a case study for Jiangsu, China. *Atmos. Chem. Phys.* 17, 7733–7756.
- Zheng, B., Huo, H., Zhang, Q., Yao, Z., Wang, X., Yang, X., Liu, H., He, K., 2014. High-resolution mapping of vehicle emissions in China in 2008. *Atmos. Chem. Phys.* 14, 9787–9805.
- Zheng, B., Tong, D., Li, M., Liu, F., Hong, C., Geng, G., Li, H., Li, X., Peng, L., Qi, J., Yan, L., Zhang, Y., Zhao, H., Zheng, Y., He, K., Zhang, Q., 2018. Trends in China's anthropogenic emissions since 2010 as the consequence of clean air actions. *Atmos. Chem. Phys.* 18, 14095–14111.